Influence of attractive forces on the solvent mediated potential of mean force between colloidal particles

S. Amokrane

Citation: The Journal of Chemical Physics **108**, 7459 (1998); doi: 10.1063/1.476166
View online: http://dx.doi.org/10.1063/1.476166
View Table of Contents: http://scitation.aip.org/content/aip/journal/jcp/108/17?ver=pdfcov
Published by the AIP Publishing

Influence of attractive forces on the solvent mediated potential of mean force between colloidal particles

S. Amokrane
Laboratoire de Physique des Milieux Désordonnés, Faculté des Sciences et de Technologie, Université Paris, 12 Val de Marne, 61 Av. du Général de Gaulle, 94010 Créteil Cedex, France

(Received 26 November 1997; accepted 30 January 1998)

The solvent induced potential of mean force between colloidal particles is computed by using the superposition approximation for the solvent–macrospheres triplet distribution function and the density functional theory for the solvent density profile at an isolated macrosphere. The influence of solute–solvent attractive forces is investigated for different diameter ratios and solvent bulk densities. For large colloidal particles, the mean force is shown to scale with the solvent–colloid hard core radius. At densities of liquid solvents, sufficient solvent–colloid attractions are found to strongly enhance the repulsive barriers in the potential of mean force and reduce the depth of the depletion well. At lower density, the mean force can become repulsive. Solvent–solvent attractions can suppress the oscillations in the potential and make it more attractive. These results are finally contrasted with those relative to purely repulsive interactions. © *1998 American Institute of Physics.* [S0021-9606(98)51917-4]

I. INTRODUCTION

Understanding how the effective interaction between solute macroparticles can be influenced by solute–solvent or solvent–solvent attractive forces remains an important question in the theory of colloids. Although some aspects of this question have already been investigated in the past (see, for example, Refs. 1 and 2 and references therein), recent studies focused on pure hard core repulsions, first because their detailed understanding is considered as a necessary step before including the effect of attractions. On the other hand, these short range repulsions can be studied *per se* because of the role of depletion forces in some colloidal suspensions.[3–5] Asymmetric hard sphere mixtures have thus been studied by various techniques, such as integral equations,[6,7] computer simulations,[8,9] density functional theory,[10] and approaches based on the entropy[11] or on the osmotic pressure.[12] Calculations predict that when the solute/solvent size ratio is sufficiently high, the depletion attraction between solutes can be strong enough to produce phase separation. This effective attraction has been invoked to explain the behavior of some suspensions in which the interactions are believed to be dominated by hard core repulsion (see, for example, the work on polystyrene spheres[13]). In addition to this well-known mechanism, the role in steric stabilization of the repulsive barriers in front of the depletion well has been emphasized in some recent studies.[14]

On the other hand, the effective interaction is found in several experiments to be strongly affected by several factors, up to the qualitative level. For instance, it was observed in Refs. 15 and 16 that changing the solvent or the temperature may turn the interaction from effective attraction to effective repulsion. Such a phase behavior, richer than that expected from purely steric effects, emphasizes the competition between entropic and enthalpic contributions, as this is well known in the theory of ordinary mixtures. The simplest studies in which attractive forces were considered and aimed at describing colloids are those based on Baxter's sticky hard sphere model[17] (SHSM). When the correlation functions are computed in the Percus–Yevick approximation (PYA) (see, e.g., Refs. 18–22), this approach is quasianalytical. It allows then a straightforward discussion of the physicochemical parameters which determine the effective interaction between the colloidal particles. In particular, Regnaut *et al.*[22] have given an analytical expression of the effective adhesiveness of very large solutes which clearly shows the crucial role played by heteroadhesions. This successful account of some trends associated with attractions between unlike species[5] confirms (see the comparison with thin square wells[23]) that the SHSM can give sensible results *when treated in the PYA* (divergences which arise in an exact treatment of the SHSM are then absent because of the particular structure of the PYA[24]). However, an important objection to the SHSM is its extreme idealization of the interaction potential, which may lead to an oversimplified picture of the real system. For example, some studies predict a gas–liquid coexistence line which changes significantly with the interaction range (see, for example, Ref. 25 for the Yukawa potential). This line does not seem to converge toward that predicted by the SHSM in the PYA since it becomes more and more flat as the attraction range decreases.

More realistic models of the interactions must be studied numerically. One can also use more sophisticated closures of the Ornstein–Zernike (OZ) equations (see, for example, Refs. 1, 2, and 26–28, and references therein) than the PYA. However, these usually require considerable computational effort, even for computing the potential of the mean force at infinite dilution. This is specially true for highly asymmetric mixtures. In this case, it is also difficult to estimate the quality of the closures since direct comparison to computer simulations exists only for hard sphere mixtures.[8,9] A simpler

approach is furnished by the superposition approximation[29] since all that is needed then is the solvent density profile at an isolated macroparticle. This scheme is well known but has not been used systematically because of the superiority of some proposed closures. While its use may not be justified if the goal is to obtain accurate results for a specific system, partial tests[8,27,28] have shown that the superposition approximation gives at least qualitatively correct results. We thus adopted it here because its computational simplicity permits us to collect a large number of data. The results of such a systematics will—in our opinion—confirm that using this approach for a qualitative purpose is indeed reasonable. The solvent density profile required for computing the superposition approximation mean force (SMF) can then be obtained by any method giving the distribution function of a fluid in an external potential, such as the density functional theory (DFT). We found Tarazona's version[30] of DFT very convenient for this purpose.

This work is organized as follows: in Sec. II, the computation of the mean force in the superposition approximation is presented, and its behavior for very large macrospheres is discussed. The computation of the DFT density profiles is detailed in Sec. III. In Sec. IV the results are finally presented and discussed.

II. POTENTIAL OF THE MEAN FORCE IN THE SUPERPOSITION APPROXIMATION

We consider a binary mixture (the solvent being component 1 and the solute component 2). We are interested in the solute's excess potential of mean force $U(r)$, at infinite dilution (its density ρ_2 goes to zero), formally defined by:

$$g_{22}(r;\rho_2\to 0)=\exp\{-\beta[u_{22}(r)+U(r)]\}, \tag{1}$$

where $g_{22}(r)$ and $u_{22}(r)$ are the pair distribution function and the direct interaction of the solutes and $\beta=1/k_BT$, T is the temperature and k_B is Boltzmann's constant. If the excess—or solvent induced—mean force $\mathbf{F}(r)$ is known, $U(r)$ can be computed as:

$$U(r)=\int_r^\infty F(x)dx. \tag{2}$$

From the formal definition of the distribution functions,[31] the mean force can be shown to be given by (see also Refs. 8 and 27):

$$\mathbf{F}(\mathbf{r})=\int \rho^{[1]}(\mathbf{r}';0,\mathbf{r})\nabla(-u_{12}(\mathbf{r}'))d\mathbf{r}', \tag{3}$$

where $u_{12}(\mathbf{r}')$ is the interaction potential between a solute at the origin and a solvent particle at $\mathbf{r}'$, and $\rho^{[1]}(\mathbf{r}';0,\mathbf{r})d\mathbf{r}'$ is the conditional probability of finding particle 1 at $\mathbf{r}'$ given that one macroparticle is at the origin and the second at $\mathbf{r}$. Kirkwood's superposition approximation[29] consists of approximating the conditional probability in Eq. (3) by $\rho^{[1]}(\mathbf{r}';0,\mathbf{r})=\rho_b g_{12}(\mathbf{r}')g_{12}(\mathbf{r}-\mathbf{r}')$, where $g_{12}(\mathbf{r})$ is the distribution function of the solvent about an isolated macrosphere and ρ_b is the solvent density far from the macrosphere ($\rho^*\equiv\rho_b d_1^3$ is the reduced density). For central potentials, the force $F(r)$ along the vector $\mathbf{r}$ can then be put in the form:

$$F(r)=\frac{\pi}{r^2}\rho_b\int_0^\infty dr'\,\frac{\partial}{\partial r'}\,u_{12}(r')g_{12}(r')H(r,r'), \tag{4a}$$

where bipolar coordinates have been used and

$$H(r,r')=\int_{|r-r'|}^{r+r'} du\; u(r^2+r'^2-u^2)h_{12}(u). \tag{4b}$$

The force being zero for a spherically symmetric distribution of the solvent about the macrospheres, $h_{12}=g_{12}-1$, has been put in place of g_{12} in the expression of $H(r,r')$. Equation (4a) can alternatively be written as

$$\beta F(r)=-\frac{\pi}{r^2}\rho_b\int_0^\infty dr'\,\frac{\partial}{\partial r'}\exp(-\beta u_{12}(r'))\times y_{12}(r')H(r,r'), \tag{4c}$$

where $y_{12}(r)=g_{12}(r)\exp(\beta u_{12}(r))$ is the cavity function. This expression is especially useful in the case of potentials with a hard core.

The force given by Eqs. (4) is an approximation of the exact force whose validity rests on that of the superposition approximation (this will be discussed in Sec. IV). It is nevertheless useful to examine its limiting behavior when the macrosphere radius $R'=0.5d_2$ and thus the solvent–solute hard core radius $R=0.5\,(d_1+d_2)$ becomes very large. Provided that $u_{12}(r)$ and hence $g_{12}(r)$ remain short ranged compared to R, this limit for separations $x=r-2R\ll R$ can be studied by using the same arguments as those invoked to obtain the planar limit of the force between macrospheres.[32,33] Omitting the details (see, for instance, Eqs. 3-1 to 3-6 in Ref. 32), Eq. (4) can be shown to give:

$$F(x)\approx\frac{\pi}{r^2}\rho_b\int_{-R}^\infty ds\,\frac{\partial}{\partial s}\,u_{12}(s+R;R)g_{12}(s+R;R)\times\int_{x-s}^\infty dt\{(s+R)^2-(t+R)^2+r^2\}(t+R)\times h_{12}(t+R;R). \tag{5}$$

Since the transformations leading to Eq. (5) are based on the conditions $|s|$, $x\ll R$, one has $t+R$, $s+R\approx R$, and the term between brackets reduces to r^2. This then cancels the denominator in front of the first integral, giving:

$$F(x;R\to\infty)=\pi R\rho_b\int_{-\infty}^\infty ds\,\frac{\partial}{\partial s}\,\bar{u}_{12}(s)\bar{g}_{12}(s)\int_{x-s}^\infty dt\;\bar{h}_{12}(t), \tag{6}$$

where a bar indicates the solvent–wall limit [it is assumed that $u_{12}(r)$ tends to a limit independent of R]. This expression shows that for macrospheres of very large radius, the SMF obeys the correct scaling with the radius (this result has been deduced numerically in Ref. 27). Such a scaling has also been obtained from the $R\to\infty$ limit of the potential of mean force in the hypernetted chain approximation (HNC). The associated mean force reads:[32,33]

$$F(x;R\to\infty)=-\pi R\rho_b\beta\int_{-\infty}^\infty ds\bar{h}_{12}(s)\bar{c}_{12}(x-s), \tag{7}$$

where $\overline{c}_{12}(s)$ is the wall–solvent direct correlation function. Equation (7) involves no superposition and can be viewed as the statistical mechanical expression of the Derjaguin approximation: $\mathrm{Lim}_{R\to\infty}(F(x,R)/\pi R)=w^{\mathrm{ex}}(x)$, where $w^{\mathrm{ex}}(x)$ is the interaction free energy per unit area between planar walls. Its generalization for including bridge functions is given in Ref. 34. Equations (6) and (7) cannot be linked in a simple way, although this could presumably be done from equations involving $\overline{c}_{12}(s)$ and $\overline{u}_{12}(s)$ such as that proposed by Lovett *et al.*[35] A simpler discussion can be made by taking the derivative of Eq. (6) with respect to x and then considering the solvent excluded region:

$$\frac{\partial}{\partial x}\left(\frac{F(x)}{\pi R}\right)=-\rho_b\int_{-\infty}^{\infty}ds\ \frac{\partial}{\partial s}\,\overline{u}_{12}(s)\overline{g}_{12}(s)\overline{h}_{12}(x-s). \tag{8}$$

If we specialize for a potential $\overline{u}_{12}(s)$ with a hard core at $s=0$, we have $\overline{g}_{12}(s)=0;\ s<0$ and $h_{12}(x-s)=-1;\ s\geqslant 0$, since $-d_1<x<0$. The right-hand side (rhs) of Eq. (8) then reads:

$$\rho_b\int_{-\infty}^{\infty}ds\ \frac{\partial}{\partial s}\,\overline{u}_{12}(s)\overline{g}_{12}(s)=k_BT_\rho(0)+\int_0^{\infty}ds\ \frac{\partial}{\partial s}\,u_{12}^{*}(s)\rho(s)=p, \tag{9}$$

where $u_{12}^{*}(s)$ is the solvent–wall potential outside the hard core, $\rho(s)=\rho_b\overline{g}_{12}(s)$ is the solvent density profile at a planar wall, and p is the bulk pressure. The second equality in Eq. (9) results from the contact value theorem[36] (a general discussion of sum rules can be found in Ref. 37). Equations (8) and (9) then give:

$$\frac{\partial}{\partial x}\left(\frac{F(x<0)}{\pi R}\right)=p. \tag{10}$$

It should be noted that the contact value theorem is known to be obeyed by the weighted density versions[38] of DFT. The result in Eq. (10) can be derived directly[32] from the exact expression of the mean force in the limit $R\to\infty$. Equation (10) shows that the slope of the SMF between macrospheres of very large radius, distant by less than one solvent diameter, would also be exact were the distribution functions $g_{12}(r)$ used to compute the mean force exact. This is rather unexpected given the approximate nature of the SMF. We found no simple explanation for this result, which shows that the terms neglected in the superposition approximation are unimportant for the slope of the mean force at large R (one possibility would be that the left-hand side (lhs) of Eqs. (6) actually equals $\pi R w^{\mathrm{ex}}(x)$ as stated by the Derjaguin approximation). Finally, Eq. (9) will serve us to check the DFT profiles $\rho(r)$ and Eq. (10) the results for the mean force. The next section gives then a brief description of the method used to compute the density profile.

III. COMPUTATION OF THE SOLVENT PROFILE IN THE DFT

The density functional theory is particularly suited for computing the solvent density profile in the external potential due to the macrosphere. We choose Tarazona's version[30] for its easy implementation and reasonable accuracy. Since this is a well-known method, details will be omitted here (a discussion of DFT can be found in the review by Evans.[38] A recent application to the adsorption at a colloid surface is given in Ref. 39).

From the general condition of minimization of the grand potential, one obtains an integral equation for the density profile which can be put in the form:

$$\rho(r)=\rho_b\ \exp\{-\beta[u_{12}(r)-\mu^{\mathrm{ex}}+f(\tilde{\rho}(r))+I^{\mathrm{att}}[\rho(r);r]+I[\tilde{\rho}(r),\rho(r);r]]\}, \tag{11a}$$

where $\mu^{\mathrm{ex}}(T,\rho_b)$ is the excess (over the ideal gas) bulk chemical potential, $\tilde{\rho}(r)$ the weighted density, $\rho(r)f(\tilde{\rho}(r))$ the reference hard sphere free energy density, taken[30] from the Carnahan–Starling equation of state,

$$I^{\mathrm{att}}[\rho(r);r]=\int d\mathbf{r}'\rho(\mathbf{r}')u^{\mathrm{att}}(\mathbf{r}-\mathbf{r}'), \tag{11b}$$

a contribution arising from the splitting of the solvent–solvent interaction potential $u_{11}(r)$ into a reference hard sphere term and an attractive part $u^{\mathrm{att}}(r)$ and

$$I[\tilde{\rho}(r),\rho(r);r]\}=\int d\mathbf{r}'\rho(r')f'(\tilde{\rho}(r'))\ \frac{\omega(\tilde{\rho}(r'),|\mathbf{r}-\mathbf{r}'|)}{1-\tilde{\rho}_1(r')-2\tilde{\rho}(r')\tilde{\rho}_2(r')} \tag{11c}$$

is a contribution associated[38] with the functional derivative $\delta\tilde{\rho}(r')/\delta\rho(r)$. The weighted density is defined by the implicit equation:

$$\tilde{\rho}(r)=\int d\mathbf{r}'\ \rho(r)\omega(\tilde{\rho}(r'),|\mathbf{r}-\mathbf{r}'|), \tag{12a}$$

where the weight function is written as $\omega(\rho,r)=\omega_0(r)+\omega_1(r)\rho+\omega_2(r)\rho^2$. The expressions of the weights $\omega_i(r)$ are given in Ref. 40. Equation (12a) can then be solved explicitly in terms of the components $\tilde{\rho}_i(r)$:

$$\tilde{\rho}_i(r)=\int d\mathbf{r}'\ \rho(r')\omega_i(|\mathbf{r}-\mathbf{r}'|), \tag{12b}$$

giving:[30,38]

$$\tilde{\rho}(r)=\frac{2\tilde{\rho}_0(r)}{1-\tilde{\rho}_1(r)+[(1-\tilde{\rho}_1(r))^2-4\tilde{\rho}_0(r)\tilde{\rho}_2(r)]^{1/2}}. \tag{12c}$$

To ensure a good numerical bulk limit of Eq. (11a), we found it convenient to replace $\rho(r')$ by $\Delta\rho(r')=\rho(r')-\rho_b$ in the term just after the integral sign in Eqs. (11b) and (11c). Then μ^{ex} no longer contains the attractive contribution and, because of the normalization of the weights ω_i, can be replaced by $\mu_{\mathrm{HS}}^{\mathrm{ex}}-\rho_b\partial f/\partial\rho=f(\rho_b)$, $\mu_{\mathrm{HS}}^{\mathrm{ex}}$ being a pure hard sphere contribution. Equation (11a) then reads:

$$\rho(r)=\rho_b\ \exp\{-\beta[u_{12}(r)+f(\tilde{\rho}(r))-f(\rho_b)+I^{\mathrm{att}}[\Delta\rho(r);r]+I[\tilde{\rho}(r),\Delta\rho(r);r]]\}. \tag{13}$$

It should finally be mentioned that the cavity function $y(r)$, being here continuous by construction, the computation of the force for hard core potentials is best handled by using Eq. (4c).

The solution of Eqs. (11)–(13) starts with an initial guess of $\rho^{\text{in}}(r)$, from which $\tilde{\rho}(r)$ [Eqs. (12b) and (12c)] and the integrals in Eqs. (11b) and (11c) are computed and a new profile $\rho^{\text{out}}(r)$ evaluated from Eq. (13). Since direct substitution is not always efficient, the input in the next iteration is taken as[30] $(1-m(r))\rho^{\text{in}}(r)+m(r)\rho^{\text{out}}(r)$. The values of the mixing function $m(r)$ which we took as a combination of two exponentials must typically be less than 0.05 at high density. At low density (up to $\rho^* \approx 0.4$), the initial profile is taken as $\rho(r)=\rho_b$, and at higher densities as the result from a previous calculation. It is also worth noting that all the integrals appearing in the solution of Eqs. (11)–(13) have the form of convolutions which are conveniently handled by Fourier transforms [a standard fast Fourier transform (FFT) algorithm for one-dimensional sine transforms was used[41]]. The analytical transform of the weights ω_i and the numerical transform of $u^{\text{att}}(r)$ are computed once for all. We found the overall structure of the computer code simpler than when the integrals are computed by direct numerical quadrature.

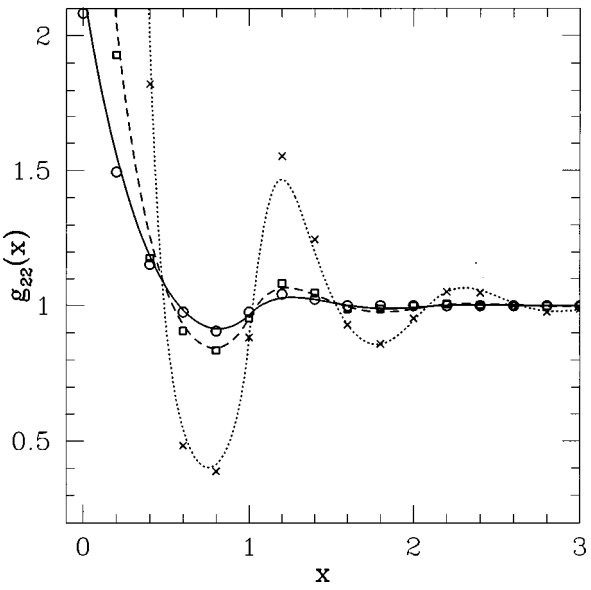

FIG. 1. Solvent induced solute pair distribution function as a function of the distance $x=r-d_2$ between the surfaces of the solutes. $d_2/d_1=1$ (full curve), 2 (dashed curve), and 10 (dotted curve). Values taken from Fig. 4 of Ref. 27 (part II) are indicated by symbols.

IV. RESULTS AND DISCUSSION

Solutes' excess potentials of mean force have been computed from Eqs. (2) and (4) and the DFT density profiles [Eq. (13)], with $u_{12}(r)$ taken as the hard sphere potential, a soft repulsive potential, a Yukawa potential, and a Lennard-Jones potential integrated over the surface of the macrosphere.[39] To simplify the discussion, most results will be given for a purely hard solvent–solvent interaction [an illustration will be given for a Lennard-Jones potential $u_{11}(r)$]. All calculations were done in double precision with d_1 taken as the unit of length, the density profiles being computed with a spacing $dr=0.01$ ($r_{\max}-r_{\min}=20$), and the mean force and the potential (which involves a triple integration) with $dr=0.02$ to reduce the CPU time (no significant difference was found with full calculations with $dr=0.01$). As is usual with hard core potentials, the functions to be Fourier transformed were smoothly extended inside the hard core by polynomials with analytical transform and, in the computation of the mean force, the contribution from $H(r,r')$ [Eq. (4b)] in the hard core was computed analytically [see Eq. (15) below].

A. Purely repulsive solute–solvent interaction

We begin with a pure hard sphere potential: $u_{12}^{hs}(r)=\infty$; $r<d_{12}$; $0r\geqslant d_{12}$. Before computing the mean force, we compared our DFT profiles to those of Henderson *et al.*[39] who also performed a Monte Carlo simulation (MC). We found no significant difference, except for the contact value. Here we find a small difference whose magnitude depends on the density. For example, for $\rho^*=0.796$ and $d_2=20d_1$, our $g_{12}(d_{12})\approx 7.13$ is about 3% higher than theirs and 6% lower than the MC value. The satisfactory comparison with MC simulation gives us some confidence that errors in the mean force will arise mostly from the superposition approximation. When computing the mean force from Eq. (4), the only contribution in the first integral comes from the discontinuity of the derivative of u_{12}^{hs} at contact. By using the continuity of the cavity function, the force can be shown to be given by:

$$\beta F(r)=\frac{\pi}{r^2}\rho_b g_{12}(d_{12})H(r,d_{12}). \tag{14}$$

When evaluating $H(r,d_{12})$, the contribution inside the hard core $[h_{12}(r<d_{12})=-1]$ was computed analytically. The corresponding result with $g_{12}(d_{12})=1$ is the Asakura–Oosawa[3] expression of the mean force.[9] Solvent induced solute distribution functions [Eq. (1) with $u_{22}^{hs}(r)$] are shown in Fig. 1 for $\rho^*=0.5$ and compared with Attard's data.[27] Attard computed the SMF from the profiles $\rho(r)$ given by the inhomogeneous Percus–Yevick approach. The good agreement observed in Fig. 1 shows that for the purpose of computing the SMF, the density profiles obtained by the two methods are of comparable quality. A more direct test is to compare the SMF with computer simulation results. In Ref. 8, it was found that the agreement with simulation is good at low density, but the SMF is too attractive near contact and the associated depletion well too deep at high density. Discrepancies at high density occur also when superposition is not used.[9] The mean force obtained with DFT profiles follows the same pattern. Figure 2 shows the result at the highest density investigated by simulation. The result for the SMF is most easily analyzed for two macrospheres at contact ($r=d_2$). The function $H(d_2,d_{12})$ can then be split as:

$$H(d_2,d_{12})=\int_{d_2-d_{12}}^{d_{12}} du\ u(d_2^2+d_{12}^2-u^2)(-1) + \int_{d_{12}}^{d_2+d_{12}} du\ u(d_2^2+d_{12}^2-u^2)h_{12}(u). \tag{15}$$

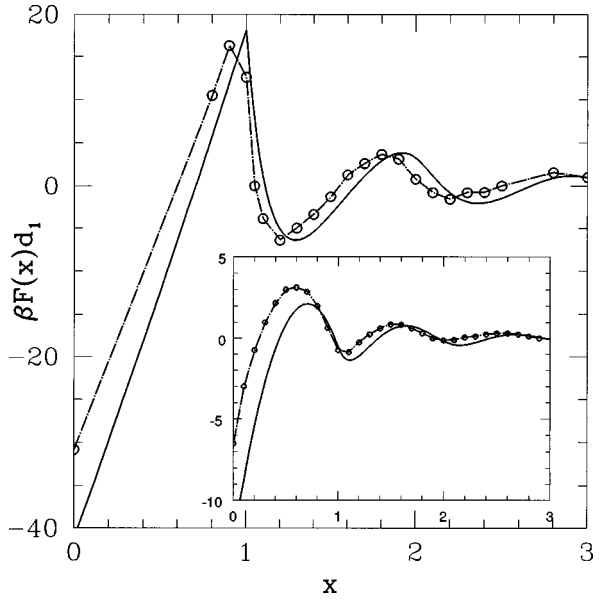

FIG. 2. Comparison of the superposition mean force (SMF) with computer simulation for $d_2/d_1=10$ and $\rho^*=0.7$. Full curve: SMF with DFT profiles. Circles: computer simulation (Ref. 8). Inset: corresponding potential of the mean force $\beta U(x)$ versus the distance $x=r-d_2$ between the surfaces of the solutes.

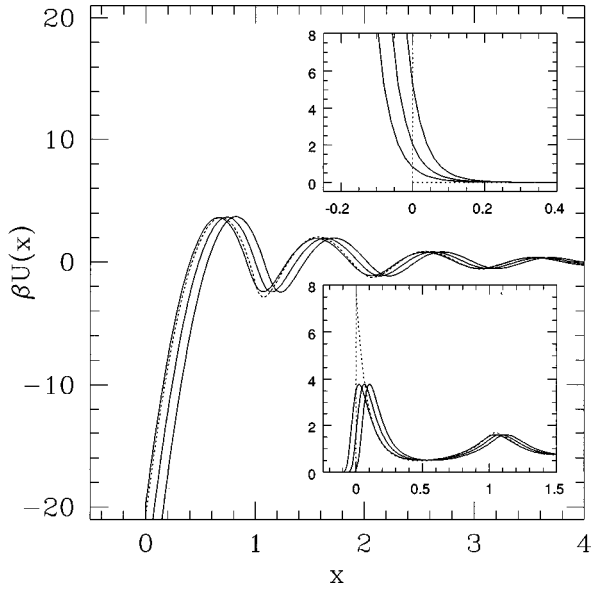

FIG. 3. Potential of the mean force computed with a soft solute-solvent repulsion: $\beta u_{12}^s(r)=0.1(r-r_0)^{-20}$ for $d_2/d_1=10$ and $\rho^*=0.835$. Full curves from left to right $r_0/d_1=4.6$, 4.64, 4.68. Dotted curve: result with u_{12}^{hs}. Upper inset: $\beta u_{12}^s(r)$, lower inset: corresponding $g_{12}(r)$.

The first integral (in the hard core) is negative and the second is positive, being dominated by the contributions near contact where the integrand is positive. The magnitude of the first integral is, however, larger (about three times for $d_2=10d_1$, mostly because $h_{12}(u)=-1$ on the range d_1, while in the second one, it drops rapidly below unity (for u greater than about $0.1d_1$). Their sum is further multiplied by the contact value $g_{12}(d_{12})$ to give a (too) negative contact force. It thus seems that the particular combination of the solvent-isolated solute distribution functions that appears in the superposition approximation overestimates the weight of the solvent excluded region. This might have some connection with Attard's observation that the superposition approximation overestimates the peaks in the triplet distribution function.[1b] This quantitative deficiency should thus be kept in mind in the discussion of the SMF. On the other hand, the slope of the force being correct for large R (see next section) suggests that a simple ansatz correcting the value of the force at contact could be sufficient.

In order to study the influence of the softness of the repulsion, we considered a repulsive potential given by $\beta u_{12}^s(r)=k(r-r_0)^{-n}$. The mean force is now given by the full expression in Eq. (4b). When $u_{12}^s(r)$ is sufficiently steep ($n\approx 20$), the only significant change from the curve $U(r)$ obtained with u_{12}^{hs} is its global shift (Fig. 3) with the effective hard core $d_{12}^{\rm eff}$ [defined, for example, such as $U(d_{12}^{\rm eff})\approx k_BT$]. In particular, the height of the first repulsive barrier is almost unaffected, despite dramatic changes in the solvent density profile. The technical reason for this can be understood from Eq. (4c). When $u_{12}^s(r)$ is sufficiently steep, $\exp(-\beta u_{12}^s(r))$ resembles more and more the unit step function and its derivative becomes sharply peaked about $r\approx d_{12}^{\rm eff}$. In contrast with $g_{12}(r)$, the cavity function $y_{12}(r)$ is very similar to that with u_{12}^{hs} and the dominant term in the integral is $\beta F(r)=(\pi/r^2)\rho_1 y_{12}(d_{12}^{\rm eff})H(r,d_{12}^{\rm eff})$. We speculate that some global constraint relating the solvent profile and the external potential, such as a force balance condition, might provide a more physical explanation of this result.

B. Solute–solvent interaction with attractive tail

The simplest way to add an attractive tail is to take $u_{12}(r)$ as a Yukawa potential:

$$\beta u_{12}^y(r)=\begin{cases}\infty, & r<d_{12}\\ \epsilon^*\dfrac{\exp(-\lambda(r-d_{12}))}{r}, & r\geqslant d_{12}\end{cases}, \tag{16}$$

in which ϵ^* controls the depth and λ the range. Equation 4 for the mean force then gives:

$$\beta F(r)=\beta\widetilde{F}_{hs}(r)+\beta\widetilde{F}_{\rm attr}(r), \tag{17}$$

where the contribution $\widetilde{F}_{hs}(r)$ associated with the discontinuity of $(\partial/\partial r')u_{12}^y(r')$ at contact is defined as in Eq. (14) and

$$\beta\widetilde{F}_{\rm attr}(r)=\frac{\pi}{r^2}\rho_b\int_{d_{12}}^{\infty}dr'\,\frac{\partial}{\partial r'}\,\beta u_{12}^y(r')g_{12}(r')H(r,r') \tag{18}$$

is the contribution outside the hard core. Of course, this splitting of the force does not correspond to a true separation of attractive and repulsive contributions since the distribution function $g_{12}(r)$ is that for the full potential. We nevertheless found it useful for analyzing the mean force.

A typical example is shown in Fig. 4(a) where the components of the force computed with u_{12}^y are compared with $F_{hs}(r)$. Near contact, $\widetilde{F}_{hs}(r)$ is more negative than $F_{hs}(r)$, essentially because $g_{12}(d_{12})$ is higher with the Yukawa interaction. The Yukawa tail indeed attracts more particles to the surface of the macrosphere, thus enhancing the packing

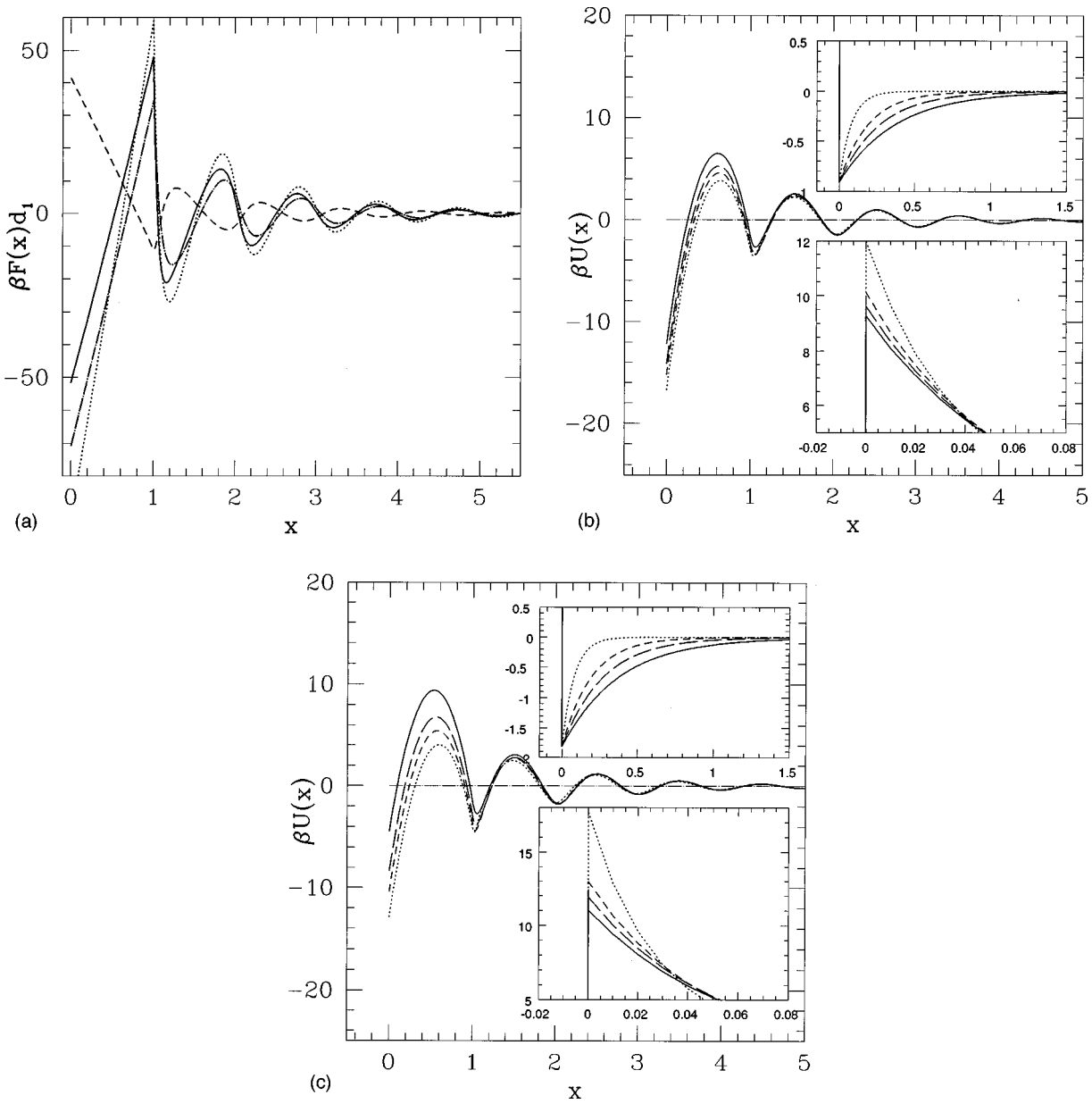

FIG. 4. (a) Components of the mean force with a Yukawa solute–solvent interaction: Dashed curve: $\widetilde{F}_{\mathrm{attr}}(r)$; dotted curve: $\widetilde{F}_{hs}(r)$; full curve: $\widetilde{F}_{\mathrm{attr}}(r)+\widetilde{F}_{hs}(r)$; dash-dotted curve: $F_{hs}(r)$ (purely hard interaction). The parameters are $d_2/d_1=10$, $\rho^*=0.835$, $\epsilon^*=10$, $\lambda=2.5$. (b) Influence of the range of the Yukawa tail for $\epsilon^*=5$. Dotted curve: $\lambda=12.5$; short dashed curve: $\lambda=5$; long dashed curve: $\lambda=3.5$; full curve: $\lambda=2.5$. Insets: upper: $u_{12}^{y}(r)$; lower: $g_{12}(r)$ near contact. The other parameters are $d_2/d_1=10$, $\rho^*=0.835$. (c) Same as Fig. 4(b) for $\epsilon^*=10$.

effect. For sufficiently large R, this can also be understood from the contact value theorem. This additional ''depletion'' contribution is, however, more than offset by the contribution $\widetilde{F}_{\mathrm{attr}}(r)$ from the tail, the total force being less attractive than with a pure hard core interaction. A noteworthy feature in Fig. 4(a) is that the slope of the total force near contact is nearly equal to that of $F_{hs}(r)$ (purely hard interaction), despite the fact that the slopes of $\widetilde{F}_{hs}(r)$ and $\widetilde{F}_{\mathrm{attr}}(r)$ are opposite and of comparable magnitude. This is numerical evidence that the trend given by Eq. (10) is already obeyed at a not too big size ratio. The influence of the range of the Yukawa tail is shown in Figs. 4(b) and 4(c) for two well depths. The overall pattern is the same in both cases, the main feature being a progressive increase of the main repulsive barrier (for $\epsilon^*=10$ and $\lambda=2.5$, the height of the barrier measured from the second minimum is about $12k_BT$). The period of the oscillations is mostly determined by the packing effect, as when the interaction is purely hard. Predicting the trend with the attraction range λ^{-1} is, however, difficult because an increase of λ^{-1} decreases the magnitude of both $\widetilde{F}_{hs}(r)$ and $\widetilde{F}_{\mathrm{attr}}(r)$ (see Table I). A possible explanation is that $|\widetilde{F}_{hs}|$ is proportional to $g_{12}(d_{12})$ and so decreases faster than $\widetilde{F}_{\mathrm{attr}}(r)$ with λ^{-1}. While the attraction between the macrosphere and one solvent particle becomes lower when λ^{-1} increases, $\widetilde{F}_{\mathrm{attr}}(r)$ indeed involves contributions from the particles in a wider interval from the macrosphere.

We mention in passing that for a square well [with range

TABLE I. Influence of the range λ^{-1} of the Yukawa potential $u_{12}^{y}(r)$ on the components of the mean force for $x=0.02d_1$, $d_2/d_1=10$, $\rho^*=0.835$, $\epsilon^*=10$. The slope of the total force is given in the fifth column (the number between parentheses is the slope computed with $u_{12}^{hs}(r)$).

λ	$\beta F_{\rm tot} d_1$	$(\beta F_{hs} d_1)$	$\beta \widetilde{F}_{\rm attr} d_1$	$\beta \widetilde{F}_{hs}(r) d_1$	$\beta F'_{\rm tot} d_1$	$(\beta F'_{hs} d_1)$
12.5	−54.67	(−68.71)	93.31	−147.98	92.70	(100.4)
5.0	−53.14	⋯	53.25	−106.39	93.85	⋯
6.5	−52.11	⋯	44.76	−96.87	94.52	⋯
2.5	−49.81	⋯	40.35	−90.17	95.07	⋯

$(\lambda-1)d_{12}]$, the force can be split as in Eq (17). $\widetilde{F}_{\rm attr}(r)$ [Eq. (18)] arises now from the discontinuity of $(\partial/\partial r')u_{12}(r')$ at $r=\lambda d_{12}$:

$$\beta \widetilde{F}_{\rm attr}(r) = -\frac{\pi}{r^2}\rho_b[g_{12}(\lambda d_{12}^-) - g_{12}(\lambda d_{12}^+)]H(r,\lambda d_{12}).$$

When λ increases, $H(d_2,\lambda d_{12})$ is expected to become more negative because $h_{12}(u)=-1$ on a longer interval [see the discussion of Eq. (15)]. Some studies[42] suggest that the discontinuity $g_{12}(\lambda d_{12}^-) - g_{12}(\lambda d_{12}^+)$ of the distribution function is either constant or decreases with λ. $\widetilde{F}_{\rm attr}(d_2)$ would thus increase in the first case but its behavior cannot be predicted in the second one. We, however, did not pursue this study since $\widetilde{F}_{\rm attr}(r)$ arises only from the somewhat artificial second discontinuity of $(\partial/\partial r')u_{12}(r')$.

Figure 5 shows the effect of the diameter ratio at a reduced density $\rho^*=0.8$. The parameters of u_{12}^{y} have been chosen so as to give the same Yukawa tail. This figure shows that the scaling [Eq. (6)] with the solute–solvent hard core radius R is obeyed to an excellent precision, even for $d_2/d_1=10$. It is worth noting that the barriers for the unscaled force can be very large, even far from contact. For $d_2=30$, for example, the barrier between the maximum at

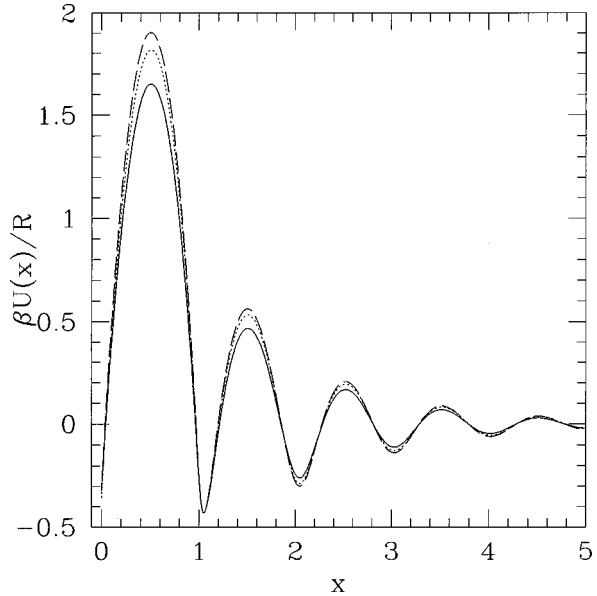

FIG. 5. Scaled potential of mean force $\beta U(x)/R$ for $\rho^*=0.8$. Full curve: $d_2/d_1=10$, $\lambda=2.5$, $\epsilon^*=10.5$; dotted curve: $d_2/d_1=20$, $\lambda=2.5$, $\epsilon^*=20$; dashed curve: $d_2/d_1=20$, $\lambda=2.5$, $\epsilon^*=30$.

TABLE II. Slope of the mean force and contact value theorem for $\rho^*=0.8$. First column: solute/solvent diameter ratio; second: slope of the mean force scaled by the solute–solvent hard core radius R. Numbers in parentheses: same with the macrosphere radius R'. third: lhs of the contact value theorem with $g_{12}(r,R<\infty)$; fourth: Carnahan–Starling solvent compressibility factor.

d_2/d_1	$\beta F'(d_2)/(\pi R\rho^*)$	$g_{12}(0)+\int_0^\infty ds\,\frac{\partial}{\partial s}u_{12}^*(s)g_{12}(s)$	$\left(\frac{\beta p}{\rho_b}\right)$CS
10	5.896 (6.485)	6.488	7.749
20	6.602 (6.933)	6.951	7.749
30	6.867 (7.096)	7.115	7.749

$r\approx 3.5\,d_1$ and the minimum at $r\approx 4\,d_1$ is about $2.25\,k_BT$. If we recall that the superposition approximation tends to lower the potential when compared to simulations, we may expect the exact barriers to be even higher. Such high repulsive barriers will, of course, have a dramatic impact on the stability of the mixture. Table II compares the slope of the mean force divided by πR [Eq. (10)], the rhs of the first equality in Eq. (9), and the bulk pressure computed from the Carnahan–Starling expression (see Ref. 27 for a similar discussion). The decrease of the difference between the first two quantities with d_2/d_1 illustrates the convergence of the slope of the force toward the large R limit in Eq. (10) (they become nearly equal if one uses the large sphere radius instead of the hard core radius R). Both differ from the bulk pressure, the difference decreasing also with d_2/d_1. The larger discrepancy at low d_2/d_1 can be attributed partly to an incomplete convergence of the profiles to the wall–particle limit (the contact theorem does not strictly apply then) and partly to the less desirable performance of DFT, as shown by comparison[39] with MC.

Figure 6 shows the effect of the density for $d_2/d_1=30$.

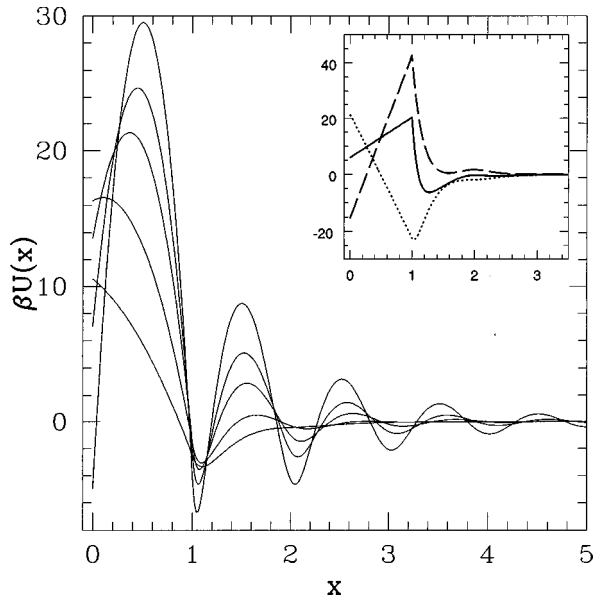

FIG. 6. Potential of the mean force $\beta U(x)$ at different densities. From top to bottom ($x\approx 0.5$): $\rho^*=0.8$, 0.7, 0.6, 0.4, 0.2. The other parameters are $d_2/d_1=30$, $\lambda=2.5$, $\epsilon^*=30$. Inset: components of the mean force for $\rho^*=0.2$. Dashed curve: $\widetilde{F}_{hs}(r)$; dotted: $\widetilde{F}_{\rm attr}(r)$; full: $\widetilde{F}_{\rm attr}(r)+\widetilde{F}_{hs}(r)$.

The increase of the magnitude of the potential with the density reflects mainly the effect of the coefficient ρ_b in front of the integral giving the force [Eqs. 4(a) and (6)]. This figure (see inset for $\rho^*=0.2$) shows also that the balance between $\tilde{F}_{hs}(r)$ and $\tilde{F}_{\text{attr}}(r)$ is strongly density dependent. At low density, the contribution of the attractive tail may become larger than that of the hard core, making the total force repulsive at contact. Although the presence of the function $H(r,r')$ in the integrand of the force complicates the discussion somehow, this trend at low ρ^* can be understood qualitatively from the behavior of $g_{12}(r)$. Except the peak at contact, $g_{12}(r)$ becomes less and less structured as the density decreases [in particular, the depleted region, $g_{12}(r)\leqslant 1$, before the second peak at $r\approx d_1$ is almost absent for $\rho^*=0.2$]. As ρ^* decreases, $g_{12}(d_{12})$ decreases and so does $\tilde{F}_{hs}(r)$, which is proportional to $g_{12}(d_{12})$. $\tilde{F}_{\text{attr}}(r)$ decreases less, especially because $g_{12}(r)$ become greater than unity almost over the entire range where $(\partial u_{12}(r)/\partial r)$ is non-negligible. As a result, the potential shows a well when the macrospheres are separated by one solvent diameter. This can be paralleled with the bridging mechanism already discussed[18,21,22] in the sticky hard sphere model. The important conclusion here is that the force between the macrospheres might become repulsive at contact, a behavior qualitatively different from that expected from a pure depletion mechanism.

In order to investigate the combined effect of an attractive tail and a soft repulsion, we finally compared the potentials of mean force obtained with the Yukawa solute–solvent interaction and an interaction obtained by integrating a Lennard-Jones potential over the surface of the macrosphere.[39] In this model, the potential felt by a solvent particle at a distance r for the center of the macrosphere is given by:

$$u_{12}^{i\text{LJ}}(r)=\int_S d^2\mathbf{r}'\left\{4\epsilon_{1g}\left[\left(\frac{\sigma_{1g}}{|\mathbf{r}-\mathbf{r}'|}\right)^{12}-\left(\frac{\sigma_{1g}}{|\mathbf{r}-\mathbf{r}'|}\right)^{6}\right]\right\}. \tag{19a}$$

The parameters of the potential are σ_{1g} and ϵ_{1g}, to keep the same notations as in Ref. 39 (actually, ϵ_{1g} combines the surface density of interacting centers on the macrosphere and the strength of the Lennard-Jones interaction between a center and a solvent particle). After integration on the azimuthal angle and a change of variables, Eq. (19a) reads

$$u_{12}^{i\text{LJ}}(r)=\frac{2\pi}{r}R'\int_{r-R'}^{r+R'}du\;u \times\left\{4\epsilon_{1g}\left[\left(\frac{\sigma_{1g}}{u}\right)^{12}-\left(\frac{\sigma_{1g}}{u}\right)^{6}\right]\right\}, \tag{19b}$$

where $R'=0.5d_2$ is the radius of the macrosphere. The analytical result is:

$$u_{12}^{i\text{LJ}}(x)=\frac{8\pi}{x+R'}R'\epsilon_{1g}\sigma_{1g}^2\{s(x+R')-s(x)\}, \tag{19c}$$

where

$$s(t)=\frac{1}{4}\left(\frac{\sigma_{1g}}{t}\right)^4-\frac{1}{10}\left(\frac{\sigma_{1g}}{t}\right)^{10} \tag{19d}$$

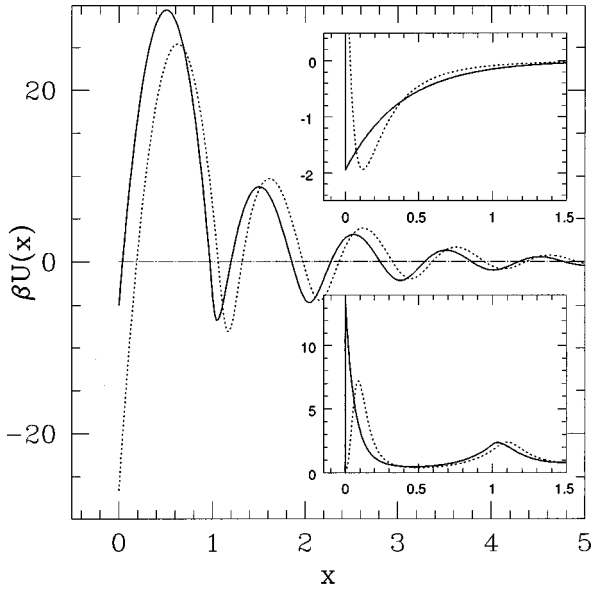

FIG. 7. Potentials of the mean force for the Yukawa and Lennard-Jones-like $u_{12}(r)$. Full curves: Yukawa with $\lambda=2.5$, $\epsilon^*=30$; dotted: integrated Lennard-Jones with $\epsilon_{1g}=1.388$, $\sigma_{1g}=0.62$. Insets: upper: $u_{12}(r)$; lower: $g_{12}(r)$. $\rho^*=0.8$; $d_2/d_1=30$.

and $x=r-R'$ is the distance of the center of the small sphere to the surface of the large one [some difference in the numerical values of $u_{12}^{i\text{LJ}}(x)$ obtained from Eqs. (19c) and (19d) and those reported in Ref. 39 appear. Whether or not $u_{12}^{i\text{LJ}}(x)$ was computed analytically in Ref. 39 with the parameters indicated is unclear to the author]. A typical result is shown in Fig. 7. The parameters of $u_{12}^{i\text{LJ}}(x)$ and of $u_{12}^{y}(x)$ were chosen so as to give the same value of $B_{12}=2\pi\int_0^\infty r^2\{1-\exp(-\beta u_{12}(r)\}dr$ which contributes to the second virial coefficients. We observe in Fig. 7 that the potentials of mean force obtained with $u_{12}^{i\text{LJ}}(x)$ and $u_{12}^{y}(x)$ are qualitatively very similar, despite the big change in the density profiles. The pattern has been found the same for $d_2/d_1=10$ and $\rho^*=0.835$. If we compare this result with that shown in Fig. 3 (see also the corresponding discussion), we may infer that the shift of $U(r)$ with $u_{12}^{i\text{LJ}}(x)$ with respect to that with $u_{12}^{y}(x)$ is essentially due to the softness of the repulsion.

C. Effect of solvent–solvent attraction

As a final illustration of the role of attractive forces, we show in Fig. 8 the potential of the mean force obtained with a solvent–solvent Lennard-Jones interaction and—to simplify the discussion—a purely hard solute–solvent potential. The solvent–solvent interaction was taken as the truncated Lennard-Jones potential:

$$u_{11}(r)=\begin{cases}4\epsilon_{11}[(d_1/r)^{12}-(d_1/r)^6]; & r\leqslant 2.5d_1\\ 0; & r>2.5d_1\end{cases}. \tag{20a}$$

$u_{11}(r)$ is further separated into the reference hard sphere part (with hard sphere diameter d_1) and an attractive part given as usual by:

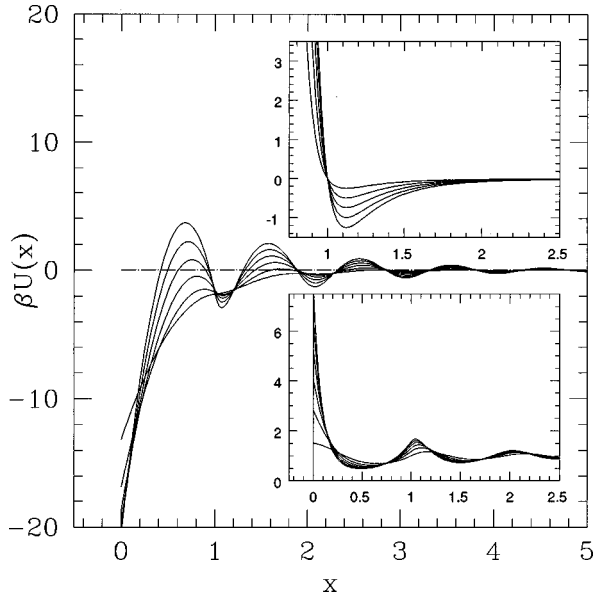

FIG. 8. Influence of the strength of the Lennard-Jones interaction on the potential of mean force. From top to bottom ($x \approx 0.5$): $\epsilon^* = 0$, 0.25, 0.5, 0.75, 1.0, 1.25. Inset: $g_{12}(r)$ (same sequence at contact). All curves are for $d_2/d_1 = 10$, $\rho^* = 0.835$.

$$u^{\mathrm{attr}}(r) = \begin{cases} -\epsilon_{11}, & r \leqslant (2d_1)^{1/6} \\ u_{11}(r), & r > (2d_1)^{1/6}. \end{cases} \tag{20b}$$

$u^{\mathrm{attr}}(r)$ in Eq. (20b) is used to evaluate the integral $I^{\mathrm{attr}}[\rho(r);r]$ [Eq. (11b)] which enters the expression of the density profile [Eqs. (11a) and (13)]. Since no solute–solvent attractions are present, the mean force is given by Eq. (14), the effect of $u^{\mathrm{attr}}(r)$ being incorporated in the change of the density profile $\rho(r)$.

The most apparent feature in Fig. 8 is the gradual damping of the oscillations in the potential of mean force as ϵ_{11} increases. This is followed by an overall downward shift of the curves, and a progressive reduction of their slope. The solvent density profile changes also dramatically as the strength of the attraction increases. These features are consequences of the lowering of the bulk pressure by the attraction. Being attracted by the bulk, the particles have a lower tendency to pack at the surface of the large sphere. $g_{12}(d_{12})$ then decreases and so does the magnitude of $\tilde{F}_{hs}(r)$ [see Eq. (14)]. This can also be understood from the contact theorem which now reads $g_{12}(d_{12}) = p/\rho_b k_B T$. This lowering of p explains the reduction of the force exerted by the small sphere and also [see Eq. (10)] the decrease of its slope near contact (not shown in Fig. 8). The damping of the oscillations can be interpreted as reflecting the progressive removal of the solvent layers between the macrospheres, which are responsible for the repulsive barriers. The overall consequence of all these features is that the force becomes negative on a wider range and $U(r)$ more attractive when the strength of the attraction increases.

This effect of solvent attractions has been studied in previous work on adhesive spheres. The potential of mean force computed[20] in the PYA shows a behavior similar to that discussed here. Solvent–solvent attractions were also found[18,20–22] to increase the solute effective adhesiveness coefficient, in qualitative agreement with the behavior of $U(r)$ found here. However, we may note, for example, that we find a significant change in the contact value $U(d_2)$ with the strength of the attraction, whereas it was found independent of the solvent adhesion in Ref. 20. Possible problems in the behavior of the mean force for sticky spheres have also been pointed out in Ref. 2, where a combination of the PY and HNC approximations was used to investigate the mean force for a nearly critical Lennard-Jones solvent. Therefore, while the SHSM in the PY approximation seems to reproduce the gross features associated with solvent attractions, some of its predictions should be regarded with caution. Finally, it should be interesting to consider in the future the combination of solute–solvent and solvent–solvent attractions, since the competition might then lead to a quite rich behavior, as suggested by our previous work[22] on the SHSM.

IV. CONCLUSION

This study has shown that while some gross structural features in the solvent induced potential of mean force between large solute particles, such as the oscillations and their periodicity, are primarily determined by hard core repulsion, they can be so strongly affected by attractive forces that the actual effective interaction may differ even qualitatively from that relative to purely repulsive forces. The appearance of strong repulsive barriers as the range of the attractions increases and the concomitant reduction of the depletion well at contact, the contact force becoming repulsive at low solvent density, and the final suppression of the oscillations by solvent–solvent attractions, indeed provide clear evidence of the importance of nonsteric interactions.

Of course, these observations are not completely new and some of them can even be deduced from models as simple as a mixture of sticky hard spheres. However, these observations—when available—were rather dispersed in the literature. In contrast, it has been possible here to deduce them from a single approach. This work then shows that the combination of the density functional theory and the superposition approximation provides an efficient tool for discussing the changes induced by attractive forces in the solvent mediated potential of mean force. However, the quantitative deficiency of the superposition approximation requires that the effect of attractions must be further investigated by more accurate analytical methods or computer simulation. Finally, the role of attractions has been investigated here at the level of the structure only. The potential of mean force can actually be used to study the thermodynamics of the mixture in an effective one-component approach. The qualitative features of the phase diagram of the effective fluid can then be investigated from available accurate techniques such as the reference hypernetted chain approximation. Such a study, which will permit the investigation of the role of enthalpic forces on properties other than the structure, is currently in progress.

ACKNOWLEDGMENT

The author is grateful to C. Regnaut for stimulating discussions.

[1] (a) P. Attard, D. Wei, G. N. Patey, and G. M. Torrie, J. Chem. Phys. **93**, 7360 (1990); (b) P. Attard, *ibid.* **95**, 4471 (1991).
[2] D. Henderson and M. Plishke, J. Chem. Phys. **97**, 7822 (1992).
[3] S. Asakura and F. Oosawa, J. Chem. Phys. **22**, 1255 (1954).
[4] W. B. Russel, D. A. Saville, and W. R. Schowalter, *Colloidal Dispersions* (Cambridge University Press, Cambridge, 1989).
[5] J. N. Israelashvili, *Intermolecular and Surface Forces* (Academic, London, (1985).
[6] T. Biben and J. P. Hansen, Phys. Rev. Lett. **66**, 2215 (1991).
[7] C. Caccamo and G. Pellicane, Physica A **235**, 149 (1997); see also C. Caccamo, Phys. Rep. **274**, 1 (1996).
[8] T. Biben, P. Bladon, and D. Frenkel, J. Phys.: Condens. Matter **8**, 10,799 (1996).
[9] R. Dickman, P. Attard, and V. Simonian, J. Chem. Phys. **107**, 205 (1997).
[10] Y. Rosenfeld, Phys. Rev. Lett. **72**, 3831 (1994).
[11] F. Saija and P. V. Giaquinta, J. Phys.: Condens. Matter **8**, 8137 (1996).
[12] H. N. W. Lekkerkerker and A. Stroobants, Physica A **195**, 387 (1993).
[13] S. Sanyal, N. Easwar, S. Ramaswamy, and A. K. Sood, Europhys. Lett. **18**, 107 (1992); A. D. Dinsmore, A. G. Yodh, and D. J. Pine, Phys. Rev. E **52**, 4045 (1995).
[14] Y. Mao, M. E. Cates, and H. N. W. Lekkerkerker, Physica A **222**, 10 (1995).
[15] C. G. de Kruif, W. J. Briels, R. P. May, and A. Vrij, Langmuir **4**, 668 (1988); C. G. de Kruif, P. W. Rouw, W. J. Briels, M. H. G. Duits, A. Vrij, and R. P. May, *ibid.* **5**, 422 (1989).
[16] M. C. Grant and W. B. Russel, Phys. Rev. E **47**, 2606 (1993).
[17] J. Baxter, J. Chem. Phys. **49**, 2770 (1968).
[18] C. Robertus, W. H. Philipse, J. H. G. Joosten, and K. Levine, J. Chem. Phys. **90**, 4482 (1989).
[19] M. H. G. M. Penders and A. Vrij, Physica A **173**, 532 (1991).
[20] A. Jamnik, D. Bratko, and D. Henderson, J. Chem. Phys. **94**, 8210 (1991).
[21] E. Dickinson, J. Chem. Soc. Faraday Trans. **88**, 3561 (1992).
[22] C. Regnaut, S. Amokrane, and Y. Heno, J. Chem. Phys. **102**, 6230 (1995).
[23] C. Regnaut and J. C. Ravey, J. Chem. Phys. **91**, 1211 (1989).
[24] G. Stell, J. Stat. Phys. **63**, 1203 (1991).
[25] E. Lomba and N. G. Almarza, J. Chem. Phys. **100**, 8367 (1994).
[26] M. Lozada-Cassou, J. Chem. Phys. **80**, 3344 (1984).
[27] P. Attard, J. Chem. Phys. **91**, 3072 (1989).
[28] M. Lozada-Cassou and E. Diaz-Herrera, J. Chem. Phys. **93**, 1386 (1990).
[29] J. G. Kirkwood, J. Chem. Phys. **3**, 300 (1935).
[30] P. Tarazona, Phys. Rev. A **31**, 2672 (1985).
[31] T. L. Hill, *Statistical Mechanics* (Dover, New York, 1987).
[32] P. Attard, D. R. Bérard, C. P. Urshenbach, and G. N. Patey, Phys. Rev. A **44**, 8224 (1991).
[33] D. Henderson, J. Chem. Phys. **97**, 1266 (1992).
[34] P. Attard and J. L. Parker, J. Phys. Chem. **96**, 5086 (1992).
[35] R. Lovett, C. Y. Mou, and F. P. Buff, J. Chem. Phys. **65**, 570 (1976).
[36] D. Henderson, L. Blum, and J. L. Lebowitz, J. Electroanal. Chem. **102**, 315 (1979).
[37] J. R. Henderson, in *Fundamentals of Inhomogeneous Fluids*, edited by D. Henderson (Marcel Dekker, New York, 1992), p. 23.
[38] R. Evans, in *Fundamentals of Inhomogeneous Fluids*, edited by D. Henderson (Marcel Dekker, New York, 1992), p. 85.
[39] D. Henderson, S. Sokolowski, and A. Patrykiejew, Mol. Phys. **85**, 745 (1995).
[40] P. Tarazona, U. Marini Bettolo Marconi, and R. Evans, Mol. Phys. **60**, 573 (1987).
[41] See fftpack and bihar directories in internet site www.netlib.org.
[42] G. Kahl and J. Hafner, Phys. Chem. Liq. **12**, 109 (1982).